

# Designing Optically Tracked Instruments for Image-Guided Surgery

Jay B. West\* and Calvin R. Maurer, Jr., *Member, IEEE*

**Abstract**—Most image-guided surgery (IGS) systems track the positions of surgical instruments in the physical space occupied by the patient. This task is commonly performed using an optical tracking system that determines the positions of fiducial markers such as infrared-emitting diodes or retroreflective spheres that are attached to the instrument. Instrument tracking error is an important component of the overall IGS system error. This paper is concerned with the effect of fiducial marker configuration (number and spatial distribution) on tip position tracking error. Statistically expected tip position tracking error is calculated by applying results from the point-based registration error theory developed by Fitzpatrick *et al.* Tracking error depends not only on the error in localizing the fiducials, which is the error value generally provided by manufacturers of optical tracking systems, but also on the number and spatial distribution of the tracking fiducials and the position of the instrument tip relative to the fiducials. The theory is extended in two ways. First, a formula is derived for the special case in which the fiducials and the tip are collinear. Second, the theory is extended for the case in which there is a composition of transformations, as is the situation for tracking an instrument relative to a coordinate reference frame (i.e., a set of fiducials attached to the patient). The derivation reveals that the previous theory may be applied independently to the two transformations; the resulting independent components of tracking error add in quadrature to give the overall tracking error. The theoretical results are verified with numerical simulations and experimental measurements. The results in this paper may be useful for the design of optically tracked instruments for image-guided surgery; this is illustrated with several examples.

**Index Terms**—Image-guided surgery, optical tracking, point-based registration, registration error, surgical instrument design.

## I. INTRODUCTION

ONE of the major features of most image-guided surgery (IGS) systems is the display of the position of a surgical probe or instrument on a preoperatively or intraoperatively acquired image of the patient. In order to accomplish this, the surgical instrument must be tracked in the physical space occupied by the patient. This task is commonly performed using an optical tracking system.<sup>1</sup> Fiducial markers, which are generally

referred to simply as fiducials, are attached to the instrument. Some instruments are specially manufactured with fiducials as a permanent part of the instrument. Many commercially available IGS systems also provide a universal tracker, which is a set of fiducials that can be attached to a generic surgical instrument. For active optical tracking, the fiducials are often light-emitting diodes, e.g., infrared-emitting diodes (IREDs). For passive optical tracking, the fiducials can be retroreflective spheres (RRSs) or disks. The instrument is then calibrated: a coordinate system is defined for the instrument and the positions of the tracking fiducials (IREDs or RRSs) and the instrument tip are determined in the instrument coordinate system.<sup>2</sup> During tracking, an optical position sensor (OPS) measures the positions of the fiducials, the measured positions (in the physical space coordinate system) are registered to the calibrated positions (in the instrument coordinate system), and the transformation obtained from this rigid point-based registration is used to map the instrument tip position to the physical space of the patient.

Often a coordinate reference frame (CRF), which is a set of tracking fiducials, is attached to the patient. For example, in cranial neurosurgery, the patient's head is frequently invasively fixed in a head clamp, and the CRF is attached via a multijointed mechanical linkage to the head clamp. In ear, nose, and throat (ENT) surgery, the CRF is generally part of a noninvasively attached head frame. In spine surgery, the CRF is often clamped to a spinous process. When a CRF is used, it defines the intraoperative coordinate system and all surgical instrument positions are reported in this coordinate system. The use of a CRF allows independent repositioning of both the patient and the OPS (e.g., to maintain an optical line of sight). Examples of optically tracked instruments and CRFs in cranial, ENT, and spine surgery can be found in [3]–[6].

<sup>2</sup>Passively tracked instruments that have posts to which RRSs are attached can be manufactured with high precision and do not need to be calibrated (personal communication, Pacific Surgical Innovations, Inc. doing business as V. Mueller Neuro/Spine, San Carlos, CA). But whereas the mechanical and optical centers of a RRS are coincident, the relationship between the mechanical and optical centers of an IRED is often variable and not necessarily known with high accuracy. Thus, actively tracked instruments manufactured with IREDs as a permanent part of the instrument are generally calibrated (personal communication, Northern Digital, Inc., Waterloo, Ontario, Canada). Calibration is also necessary for generic instruments with universal trackers. The calibration is a two-step process. First, a coordinate system is defined for the instrument (or universal tracker) and the positions of the fiducials are determined in the instrument (or tracker) coordinate system. Second, the position of the instrument tip is determined in the instrument (or tracker) coordinate system. For instruments with permanently attached fiducials, both steps are generally performed by the manufacturer. For generic instruments with temporarily attached universal trackers, the first step is performed by the manufacturer and the second step is performed by the user. For instruments with permanently attached fiducials, the second step is sometimes performed by the user as a quality control procedure (e.g., to safeguard against the possibility of a bent tip).

Manuscript received January 7, 2004. The Associate Editor responsible for coordinating the review of this paper and recommending its publication was P. Cinquin. *Asterisk indicates corresponding author.*

\*J. B. West is with Accuray, Inc., 1310 Chesapeake Terrace, Sunnyvale, CA 94089 USA (e-mail: jwest@accuray.com).

C. R. Maurer, Jr. is with the Image Guidance Laboratories, Department of Neurosurgery, Stanford University, Stanford, CA 94305 USA (e-mail: calvin.maurer@igl.stanford.edu).

Digital Object Identifier 10.1109/TMI.2004.825614

<sup>1</sup>The idea of optically tracking an object by attaching light emitters or reflectors is at least 20 years old [2]. Several optical tracking systems are commercially available. Although a variety of instrument tracking methods have been used in IGS systems, including mechanical, acoustic, and magnetic tracking systems, almost all current commercially available IGS systems track surgical instruments using an optical tracking system.

Instrument tracking error is an important component of the overall IGS system error (see [7] for a detailed discussion of various sources of error). Accuracy measurements have been reported for optically tracked instruments using a variety of OPSs [8]–[10]. These measurements were performed for instruments with a fixed fiducial marker configuration (number and spatial distribution). This paper is concerned with the effect of fiducial marker configuration on tip position tracking error. Statistically expected tip position tracking error is calculated by applying results from the point-based registration error theory developed by Fitzpatrick *et al.* [11]. Tracking error depends not only on the error in localizing the fiducials, which is the error value generally provided by manufacturers of optical tracking systems, but also on the number and spatial distribution of the tracking fiducials and the position of the instrument tip relative to the fiducials. A formula for the special case of collinear fiducials is derived. The theory is extended to the case in which there is a composition of transformations, as is the situation for tracking an instrument relative to a CRF, and we use this result to compute tip position tracking error for a variety of positions of an instrument tip relative to a CRF. Finally, the theoretical results are verified with numerical simulations and experimental measurements.

## II. THEORY

### A. Review of Point-Based Registration Error Theory

The rigid point-based registration problem is generally defined to be the problem of finding the rotation matrix and the translation vector that aligns one set of  $N$  points  $\{\mathbf{x}_i\}$  with a corresponding set  $\{\mathbf{y}_i\}$ ,  $i = 1, 2, \dots, N$ , such that the distance between corresponding points is minimized in the root-mean-square (rms) sense. The problem reduces to finding the rotation matrix  $R$  and translation vector  $\mathbf{t}$  that minimizes the mean-square distance

$$d^2 = \frac{1}{N} \sum_{i=1}^N |\mathbf{y}_i - (R\mathbf{x}_i + \mathbf{t})|^2. \quad (1)$$

If  $d = 0$ , the fiducial registration is perfect. Typically, however, because of errors in localizing the fiducials, the fit is only approximate. The optimal translation is given by

$$\mathbf{t} = \bar{\mathbf{y}} - R\bar{\mathbf{x}} \quad (2)$$

where the bar indicates the mean value of the point set [12]. Calculation of the optimal rotation is a bit more difficult because of the nonlinear constraint that the rotation matrix be orthogonal. The first solution was published by Schönemann [13]. Many others have produced independent solutions of the problem, including several that represent rotations by orthogonal matrices and use singular value decomposition [14]–[16] (these are equivalent to Schönemann's solution [17]) and several that represent rotations by unit quaternions [18]–[20]. A recent comparison of these methods, plus a method based on the matrix square root [21], [22] and another method based on dual number quaternions [23], evaluated their numerical accuracy and stability and concluded that there are no substantial differences among them [24].

There are several types of errors associated with point-based registration [7], [11], [25], [26]:

- *Fiducial localization error* (FLE) is the distance between the true position of a fiducial and its measured position, i.e., the error of localizing the fiducial. In the case of optically tracked instruments, FLE is the error the optical tracking system makes when it measures the position of a fiducial marker attached to the surgical instrument in the physical space coordinate system of the OPS.
- *Fiducial registration error* (FRE) is the distance between corresponding fiducial points after registration. In the case of optically tracked instruments, the tracking system aligns the measured positions of the fiducial markers attached to the surgical instrument in the physical space coordinate system of the OPS with the known (calibrated) positions of the fiducial markers in the instrument coordinate system; FRE is the residual distance between corresponding fiducial positions after this alignment.
- *Target registration error* (TRE) is the distance between corresponding points other than the fiducial points after registration. In the case of optically tracked instruments, the tracking system uses the transformation obtained by aligning the measured and known (calibrated) fiducial marker positions to map the instrument tip position from the instrument coordinate system to the physical space coordinate system of the OPS; TRE, which is the error of this mapping, is the tip position tracking error.

These errors are illustrated in Fig. 1. Although FLE, FRE, and TRE are actually vector quantities, they are generally reported as scalar values that are the lengths of the vectors. The quantity FLE is normally used to mean the statistical rms average of the localization error, which is the square root of its expected squared value, that is,  $\text{rms}[\text{FLE}] = \sqrt{\langle \text{FLE}^2 \rangle}$ , where  $\langle \cdot \rangle$  denotes expected value. The quantity FRE can refer to the registration error of an individual fiducial, in which case a subscript is added. Without a subscript, FRE is normally used to mean the rms average of the individual registration errors. The rms FRE is the minimum value of the rms distance  $d$  in the cost function in (1). The quantity TRE depends on the position of the target point. Generally  $\text{TRE}(\mathbf{r})$  is used to denote the registration error at the position  $\mathbf{r}$ .

Consider a set of  $N$  fiducial points that is registered to another set of points that differs from the first set by position, orientation, and noise that is added to each point (identical, independent, zero-mean, isotropic, normally distributed noise). Let  $\sigma^2$  be the variance of the coordinate components of the random noise. In our case, the random noise represents the error of determining the positions of the fiducial markers. Thus,  $\sigma^2 = \langle \text{FLE}^2 \rangle / 3$ , and  $\text{rms}[\text{FLE}] = \sqrt{3\sigma^2}$ . Sibson [27] showed using perturbation theory that if the points are registered in a least-squares sense using a rigid transformation, then  $\text{FRE}^2 \sim \sigma^2 \chi_{3N-6}^2$ . This means that for a particular localization error (i.e., a particular value of  $\text{rms}[\text{FLE}]$ , or equivalently, a particular value of  $\sigma$ ), there is a statistical distribution of FRE values for which the probabilities are given by the chi-square ( $\chi^2$ ) distribution with  $3N - 6$  degrees of freedom. It can be shown from this probability distribution that there is a statistical

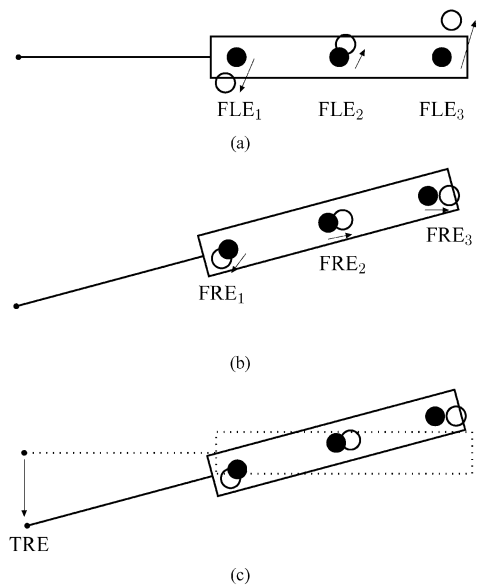


Fig. 1. Illustration of several types of error associated with point-based registration. (a) FLE is the distance between the true position (solid circles) of a fiducial and its measured position (open circles), i.e., the error of localizing the fiducial. In the case of optically tracked instruments, FLE is the error the optical tracking system makes when it measures the position of a fiducial marker attached to the surgical instrument in the physical space coordinate system of the OPS. (b) FRE is the distance between corresponding fiducial points after registration. In the case of optically tracked instruments, the tracking system aligns the measured positions of the fiducial markers attached to the surgical instrument in the physical space coordinate system of the OPS with the known (calibrated) positions of the fiducial markers in the instrument coordinate system; FRE is the residual distance between corresponding fiducial positions after this alignment. (c) TRE is the distance between corresponding points other than the fiducial points after registration. In the case of optically tracked instruments, the tracking system uses the transformation obtained by aligning the measured and known (calibrated) fiducial marker positions to map the instrument tip position from the instrument coordinate system to the physical space coordinate system of the OPS; TRE, which is the error of this mapping, is the tip position tracking error. In the case of an optically tracked instrument, the fiducials are the infrared-emitting diodes or retroreflective spheres attached to the instrument, the two fiducial point sets are the calibrated fiducial positions in the instrument coordinate system and the corresponding measured fiducial positions in the world coordinate system of the optical tracking system, the target  $\mathbf{r}$  is the tip of the instrument, and  $\text{TRE}(\mathbf{r})$  is the tip position tracking error.

relationship among the expected value of FRE, FLE, and the number of fiducials  $N$ , which is described by

$$\langle \text{FRE}^2 \rangle = \frac{N-2}{N} \langle \text{FLE}^2 \rangle. \quad (3)$$

The expected value of FRE depends only on the expected value of FLE and the number of fiducials  $N$ , and is independent of the spatial distribution of the fiducials.

Fitzpatrick *et al.* [11], [28] recently showed using perturbation theory that there is a statistical relationship among the expected value of TRE, FLE, the number of fiducials  $N$ , the spatial distribution of the fiducials, and the position of the target relative to the fiducials, which is described by

$$\langle \text{TRE}^2(\mathbf{r}) \rangle = \frac{\langle \text{FLE}^2 \rangle}{N} \left( 1 + \frac{1}{3} \sum_{k=1}^3 \frac{d_k^2}{f_k^2} \right) \quad (4)$$

where  $d_k$  is the distance of the target point  $\mathbf{r}$  from the  $k$ th principal axis of the fiducial point set, and  $f_k$  is the rms distance of the fiducials from the  $k$ th axis ( $f_k$  is effectively the radius

of gyration of the fiducial set about its  $k$ th principal axis). The constant inside the parentheses in (4) represents the translational component of TRE; the summation term represents the rotational component. Several observations about the nature of the statistically expected value of TRE can be made based on inspection of (4): 1) TRE (both its value at a particular position as well as its average over a region of interest) is proportional to  $\text{rms}[\text{FLE}]$ . 2) TRE is inversely proportional to  $\sqrt{N}$ , assuming that fiducials are added to the configuration such that their rms distance to the three principal axes ( $f_k$ ) remains constant. 3) TRE depends on the position  $\mathbf{r}$  of the target point. 4) TRE has its minimum value at the fiducial configuration centroid, and that value, which is  $\text{rms}[\text{FLE}]/\sqrt{N}$ , is purely the translational component of registration error. 5) TRE increases as the distance of the target point from the principal axes increases. 6) The iso-error TRE contours are ellipsoidal. These observations are consistent with many published results [25], [29]–[31].

### B. Application to Optically Tracked Instruments

Point-based registration error theory was originally developed for analyzing and predicting the image-to-physical registration accuracy of IGS systems that align preoperative images with the physical space occupied by the patient using anatomical landmarks, skin-affixed markers, or bone-implanted markers [11], [28]. It has been applied to develop guidelines for fiducial marker placement in cranial IGS [7], [26]. In this case, the points  $\{\mathbf{x}_i\}$  are the localized fiducial marker positions in the image coordinate system, the points  $\{\mathbf{y}_i\}$  are the corresponding localized fiducial positions in the physical coordinate system, and  $\text{TRE}(\mathbf{r})$  is the registration error at a particular anatomical position  $\mathbf{r}$ . The word “target” was originally used to help distinguish the quantity TRE from FRE and in the context of IGS was picked to suggest that the anatomical position is a surgical target (e.g., a tumor) [25].

Point-based registration error theory can also be usefully applied to the design of optically tracked instruments, which are commonly used in IGS. In the case of an optically tracked instrument, the points  $\{\mathbf{x}_i\}$  are the calibrated tracking fiducial marker positions in the instrument coordinate system, the points  $\{\mathbf{y}_i\}$  are the corresponding measured fiducial positions in the world coordinate system of the optical tracking system, the target  $\mathbf{r}$  is the tip of the instrument, and  $\text{TRE}(\mathbf{r})$  is the tip position tracking error. This application assumes that the optical tracking system is solving (1) and that the fiducial measurement error is identical, independent, zero-mean, and isotropic. Some optical tracking systems provide the measured fiducial positions and the user can compute the instrument-to-world transformation using (1). Other systems compute the transformation internally and the user does not generally have documentation about the algorithm used. Generally FLE is slightly anisotropic, with error along the optical axis of the OPS higher than error perpendicular to this axis. Also, the optical center of IREDs used for active optical tracking is slightly angle dependent. Thus, some of the assumptions of point-based registration error theory are only approximately true in the application of the theory to optically tracked instruments. One of the goals of this work is to evaluate the accuracy of theoretical predictions of instrument tip position tracking error.

### C. Special Case of Collinear Fiducials

Solutions to the rigid-body registration problem [13], [15], [16] do not take into account the case in which the fiducial configuration is described by an object of dimension  $K - 2$ , where  $K$  is the spatial dimension. In three-dimensional (3-D) space ( $K = 3$ ), this is the case in which the fiducials are collinear. In this situation there is no unique solution to the registration problem, because a rotation about the line of the fiducials does not change their positions, and hence does not change FRE. Thus, it is also clear that, when the target is not on the same line as the fiducials, any attempt to derive TRE is pointless, because TRE can be changed by altering the arbitrary rotation parameter in the registration transform. However, it is possible to extend the TRE analysis of Fitzpatrick *et al.* [11], [28] to the case in which the fiducials and the target all lie on a common line  $L$ . This case is practically important because many commercially available IGS systems include a tracked pointer probe with collinear fiducials.

Following the analysis in [11], we align the coordinate axes with the principal axes of the fiducial configuration, and set the origin to be its centroid. In this case, there is only one axis corresponding to a nonzero eigenvalue; this axis is the line  $L$ . The other two axes may be chosen in any way provided that they are perpendicular to each other and to  $L$ . Because the axes may be labeled arbitrarily, without loss of generality we assume that the fiducials and target all lie on the  $x$  axis, i.e.,  $L$  is the line  $y = z = 0$ . The registration problem is solved for the rotation  $R$  and translation  $\mathbf{t}$ , where  $\mathbf{t}$  is well defined, and  $R$  is defined up to the arbitrary rotation angle about  $L$ . Using the perturbation theory approach employed by Fitzpatrick [11], to a first-order approximation, the translational component of the rigid transformation, and the rotational components about the  $y$  and  $z$  axes, are not affected by the collinearity of the fiducials. The coordinates of transformed points that lie on the  $x$  axis are unaffected by any rotation about the  $x$  axis, so we may ignore any such rotation. Thus, the TRE measured at a point  $\mathbf{r} = (\rho, 0, 0)^t$  may be written as the usual translational component plus the  $y$  and  $z$  rotational components of TRE in the noncollinear case. Because all of the fiducials lie on the  $x$  axis, (4) simplifies to

$$\langle \text{TRE}^2(\mathbf{r}) \rangle = \frac{\langle \text{FLE}^2 \rangle}{N} \left( 1 + \frac{2\rho^2}{3f^2} \right) \quad (5)$$

where  $\rho = d_y = d_z$  and  $f = f_y = f_z$ .

### D. Composition of Transformations

The original development of point-based registration error theory is concerned with the case in which a single point-based registration is performed, e.g., the registration of the calibrated fiducial positions in the instrument coordinate system to the corresponding measured fiducial positions in the world coordinate system of the optical tracking system. In order to track a surgical probe or instrument relative to a CRF, two point-based registrations are performed. Transformations relating both the instrument coordinate system and the CRF coordinate system to the world coordinate system of the optical tracking system are computed. These two transformations are composed (i.e., applied

serially) in order to find the transformation relating the instrument coordinate system to that of the CRF. An extension of TRE theory is necessary in order to account for this composition.

In the algebra that follows, bold type indicates vector quantities, and italic type indicates scalars and matrices. The goal of tracking is to measure the position of the instrument's tip in the coordinate frame of the CRF. This estimate is denoted as  $\mathbf{p}_c$ . An asterisk denotes exact values (e.g., the true positions of the fiducials in physical space), and the absence of an asterisk denotes estimated values (e.g., the positions of these fiducials as measured by the OPS). We assume that we have a perfect model of the instrument, i.e., the positions of the fiducial points and the position of the tip are known exactly in the instrument's own coordinate system. We are concerned here only with 3-D space ( $K = 3$ ). The  $N \times 3$  matrix containing the  $N$  fiducial positions in instrument space is denoted as  $F_i$ , and the tip position in this space as  $\mathbf{p}_i$ . Because of the assumption that the model of the instrument is perfect,  $F_i \equiv F_i^*$  and  $\mathbf{p}_i \equiv \mathbf{p}_i^*$ . The exact positions of the fiducials measured in physical space by the OPS are related to  $F_i^*$  by a rigid transformation. We write these positions as  $F_p^*$ , and the transformation mapping  $F_i^*$  to  $F_p^*$  as  $\mathcal{T}_{ip}^*$ . This transformation also maps the tip position from instrument space to physical (OPS) space, i.e.,

$$\mathbf{p}_p^* = \mathcal{T}_{ip}^*(\mathbf{p}_i^*) = \mathcal{T}_{ip}^*(\mathbf{p}_i). \quad (6)$$

However, because of localization error in physical space, the measured positions  $F_p$  of the fiducials in physical space do not perfectly match the exact positions  $F_p^*$ . Hence we must find a registration transformation  $\mathcal{T}_{ip}$  that is an estimate of  $\mathcal{T}_{ip}^*$ , the exact transformation from instrument to physical space. The most common way to do this is to find the rotation and translation that minimizes FRE (i.e., solves (1)), and the TRE theory developed by Fitzpatrick *et al.* [11], [28] assumes that this registration approach is used. Using any of the registration methods cited in Section II-A, we have that

$$\mathbf{p}_p = \mathcal{T}_{ip}(\mathbf{p}_i). \quad (7)$$

By definition, the TRE vector at the tip position  $\mathbf{p}_p$  is

$$\mathbf{TRE}_{ip}(\mathbf{p}_p) = \mathcal{T}_{ip}(\mathbf{p}_i) - \mathcal{T}_{ip}^*(\mathbf{p}_i) = \mathbf{p}_p - \mathbf{p}_p^*. \quad (8)$$

The subscript "ip" on the quantity  $\mathbf{TRE}_{ip}(\mathbf{p}_p)$  denotes the error introduced by the transformation from instrument to physical space; we later use the subscript "pc" to denote the error introduced by the registration from physical to CRF space. In order to calculate  $\mathbf{p}_c$ , we must perform a second registration. The positions of the CRF fiducials in the coordinate frame of the CRF are denoted as  $C_c$ . Again we assume that the model of the CRF is perfect, so that  $C_c \equiv C_c^*$ . We write the positions of the CRF's fiducials as measured by the OPS in physical space as  $C_p$ , and we calculate the transformation  $\mathcal{T}_{pc}$  that best maps  $C_p$  to  $C_c$ . Since this transformation also maps the tip position from physical space to CRF space

$$\mathbf{p}_c = \mathcal{T}_{pc}(\mathcal{T}_{ip}(\mathbf{p}_i)) = \mathcal{T}_{pc}(\mathbf{p}_p). \quad (9)$$

Using the definition of  $\mathbf{TRE}_{ip}(\mathbf{p}_p)$

$$\begin{aligned} \mathbf{p}_c^* &= \mathcal{T}_{pc}^*(\mathcal{T}_{ip}^*(\mathbf{p}_i^*)) = \mathcal{T}_{pc}^*(\mathbf{p}_p^*) \\ &= \mathcal{T}_{pc}^*(\mathbf{p}_p - \mathbf{TRE}_{ip}(\mathbf{p}_p)) \end{aligned} \quad (10)$$

and, thus

$$\begin{aligned} \mathbf{TRE}(\mathbf{p}_c) &= \mathbf{p}_c - \mathbf{p}_c^* \\ &= \mathcal{T}_{pc}(\mathbf{p}_p) - \mathcal{T}_{pc}^*(\mathbf{p}_p^*) \\ &= \mathcal{T}_{pc}(\mathbf{p}_p) - \mathcal{T}_{pc}^*(\mathbf{p}_p - \mathbf{TRE}_{ip}(\mathbf{p}_p)) \\ &= \mathbf{TRE}_{pc}(\mathbf{p}_c) + \mathcal{T}_{pc}^*(\mathbf{TRE}_{ip}(\mathbf{p}_p)) \end{aligned} \quad (11)$$

where

$$\mathbf{TRE}_{pc}(\mathbf{p}_c) = \mathcal{T}_{pc}(\mathbf{p}_p) - \mathcal{T}_{pc}^*(\mathbf{p}_p). \quad (12)$$

Because  $\mathbf{TRE}$  represents a difference vector rather than a spatial position, the transformation  $\mathcal{T}_{pc}^*$  applied to  $\mathbf{TRE}_{ip}$  consists only of a rotation. Thus, the expected squared magnitude may be written as

$$\begin{aligned} \langle \mathbf{TRE}^2(\mathbf{p}_c) \rangle &= \langle \mathbf{TRE}_{pc}^2(\mathbf{p}_c) \rangle + \langle \mathbf{TRE}_{ip}^2(\mathbf{p}_p) \rangle \\ &\quad + 2\langle \mathbf{TRE}_{pc}(\mathbf{p}_c) \cdot \mathcal{T}_{pc}^*(\mathbf{TRE}_{ip}(\mathbf{p}_p)) \rangle. \end{aligned} \quad (13)$$

Fitzpatrick *et al.* [28] showed that  $\mathbf{TRE}$  can be decomposed into three orthogonal components that have independent, zero-mean, normal distributions. Thus, the dot product in (13) may be written as a sum of products of independent, zero-mean variables and the expected value of the dot product is zero. This allows the simplification of (13) to

$$\langle \mathbf{TRE}^2(\mathbf{p}_c) \rangle = \langle \mathbf{TRE}_{ip}^2(\mathbf{p}_p) \rangle + \langle \mathbf{TRE}_{pc}^2(\mathbf{p}_c) \rangle. \quad (14)$$

In summary, the expected squared TRE for a serial composition of transformations is the sum of the expected squared TREs for the individual transformations. The terms on the right side of (14) can be computed using (4). For the case of a surgical probe or instrument tracked relative to a CRF, the first term is computed using the tip position relative to the instrument fiducials in the coordinate frame of the instrument; the second term is computed using the tip position relative to the CRF fiducials in the coordinate frame of the CRF.

### E. Examples

The tip position tracking error ( $\mathbf{TRE}_{ip}$ ) of an optically tracked instrument can be computed using (4), or (5) if the fiducial markers are collinear with the tip. For simple fiducial geometries, it is possible to derive analytical expressions in terms of  $\langle \mathbf{FLE}^2 \rangle$  and geometrical parameters describing the fiducial configuration. Five examples of instruments with various fiducial configurations are illustrated in Fig. 2. The expected squared tip position tracking error is the sum of a translational component, which is  $\langle \mathbf{FLE}^2 \rangle / N$ , and a rotational component, which is

$$\langle \mathbf{TRE}^2(\mathbf{r}) \rangle_{\text{rotation}} = \frac{\langle \mathbf{FLE}^2 \rangle}{3N} \sum_{k=1}^3 \frac{d_k^2}{f_k^2}. \quad (15)$$

The rotational component of the tip position tracking error is listed in Table I for the five instruments shown in Fig. 2. The rotational component of error is much greater than the translational component; the error of approximating the tip position tracking error by its rotational component is typically less than 10%, and often less than 5%, for practical choices of  $\rho$ ,  $A$ , and  $B$  for the instruments shown in Fig. 2.

Optically tracked instruments tend to have fiducial configurations with considerable anisotropy. In particular,  $f_x$  is generally

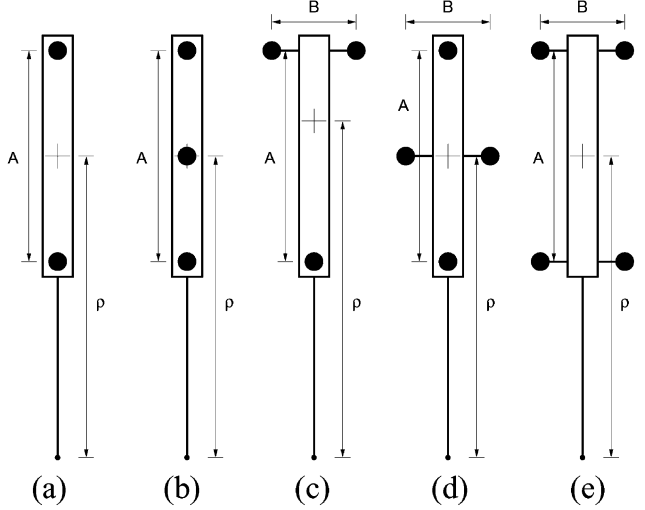


Fig. 2. Optically tracked instruments with various fiducial marker configurations. The fiducial markers, which are shown here as large solid circles, can be infrared-emitting diodes or retroreflective spheres. The instrument tip is shown as a small solid circle. The centroid of the fiducial configuration is shown as a cross. The parameters  $A$  and  $B$  are distances between fiducials;  $\rho$  is the distance from the instrument tip to the fiducial centroid. (a) Two fiducials that are collinear with the tip. (b) Three equally spaced fiducials that are collinear with the tip. (c) Three fiducials arranged in a triangle. (d) Four fiducials arranged in a cross. (e) Four fiducials arranged in a rectangle.

TABLE I  
TIP POSITION TRACKING ERROR FOR INSTRUMENTS WITH VARIOUS FIDUCIAL CONFIGURATIONS

Case	Configuration	$N$	Rotational Component
a	Line	2	$\frac{4}{3} \frac{\rho^2}{A^2} \langle \mathbf{FLE}^2 \rangle$
b	Line	3	$\frac{4}{3} \frac{\rho^2}{A^2} \langle \mathbf{FLE}^2 \rangle$
c	Triangle	3	$\frac{8+3\xi^2}{2(4+3\xi^2)} \frac{\rho^2}{A^2} \langle \mathbf{FLE}^2 \rangle$
d	Cross	4	$\frac{2(2+\xi^2)}{3(1+\xi^2)} \frac{\rho^2}{A^2} \langle \mathbf{FLE}^2 \rangle$
e	Rectangle	4	$\frac{2+\xi^2}{3(1+\xi^2)} \frac{\rho^2}{A^2} \langle \mathbf{FLE}^2 \rangle$

Case refers to instrument fiducial configurations illustrated in Fig. 2. Configuration refers to the geometrical arrangements of the  $N$  fiducials. Rotational Component is the rotational component of the expected squared TRE at the instrument tip. The translational component is  $\langle \mathbf{FLE}^2 \rangle / N$ . The parameters  $\rho$ ,  $A$ , and  $\xi = B/A$  refer to the distances defined in Fig. 2.

zero or small, where  $x$  is the principal axis corresponding to the axis of the instrument. Since the primary concern is tracking the tip of the instrument, and since the tip is either on or near the  $x$  axis, the ratio  $d_x/f_x$  is either zero or small. However, because there is considerable variability in the positioning of a CRF in an operating room environment, and because an instrument needs to be tracked over a volume (rather than along an axis), a CRF cannot have any small values of  $f_k$ , otherwise the ratio  $d_k/f_k$  will be large in some situations, and, as can be seen by inspection of (4), a large value of the ratio  $d_k/f_k$  will cause a large tracking error. Thus, fiducial configurations such as those shown in Fig. 2 are poor choices for a CRF.

Consider  $N$  fiducials equally spaced on a circle of radius  $r$  centered at the origin in the  $xy$  plane, e.g., three fiducials arranged in an equilateral triangle or four fiducials arranged in a

TABLE II  
TRACKING ERROR FOR CRFs WITH SIMPLE FIDUCIAL CONFIGURATIONS

Configuration	Rotational Component
Regular polyhedron	$\frac{2}{3} \frac{\rho^2}{r^2} \frac{\langle \text{FLE}^2 \rangle}{N}$
Regular polygon, $\phi = 0$	$\frac{\rho^2}{r^2} \frac{\langle \text{FLE}^2 \rangle}{N}$
Regular polygon, $\phi = \pi/2$	$\frac{4}{3} \frac{\rho^2}{r^2} \frac{\langle \text{FLE}^2 \rangle}{N}$

*Configuration* refers to the geometrical arrangement of the  $N$  fiducials. The fiducials are placed at the vertices of the geometrical objects listed, e.g., at the vertices of a regular tetrahedron for  $N = 4$  or an equilateral triangle for  $N = 3$ . *Rotational Component* is the rotational component of the expected squared TRE at a target (e.g., an instrument tip). The translational component is  $\langle \text{FLE}^2 \rangle / N$ . The parameter  $\rho$  is the distance of the target from the fiducial centroid and  $r$  is the distance of the fiducials from the fiducial centroid (i.e., the radius of the sphere or circle circumscribing the regular polyhedron or polygon, respectively). For the regular polygon,  $\phi$  is the angle between the target  $\mathbf{r}$  and the plane of the fiducials;  $\phi = 0$  corresponds to navigating within the plane of the CRF,  $\phi = \pi/2$  corresponds to navigating perpendicular to the plane.

square. In this case,  $f_x = f_y = r/\sqrt{2}$  and  $f_z = r$ . For a target  $\mathbf{r} = (x, y, z)$ ,  $d_x^2 = y^2 + z^2$ ,  $d_y^2 = x^2 + z^2$ , and  $d_z^2 = x^2 + y^2$ . The summation term in (4) is  $\sum_k d_k^2 / f_k^2 = (3x^2 + 3y^2 + 4z^2) / r^2 = (3 + \sin^2 \phi) \rho^2 / r^2$ , where  $\rho = \sqrt{x^2 + y^2 + z^2}$  is the distance of the target from the fiducial centroid and  $\phi = \sin^{-1} z / \rho$  is the angle between  $\mathbf{r}$  and the fiducial plane. The expected squared TRE( $\mathbf{r}$ ) described by (4) reduces to a fairly simple equation of FLE,  $N$ ,  $\rho/r$ , and  $\phi$

$$\langle \text{TRE}^2(\mathbf{r}) \rangle = \frac{\langle \text{FLE}^2 \rangle}{N} \left( 1 + \frac{3 + \sin^2 \phi}{3} \frac{\rho^2}{r^2} \right). \quad (16)$$

The ratio  $(3 + \sin^2 \phi) / 3$  varies from 1 (for  $\phi = 0$ ) to  $4/3$  (for  $\phi = \pi/2$ ). A value of  $\phi = 0$  corresponds to navigating within the plane of the CRF fiducials; a value of  $\phi = \pi/2$  corresponds to navigating perpendicular to the plane. Thus, the TRE at a point relative to a planar array of fiducials arranged in a regular polygon is dependent on orientation, but the dependence is small, and such a fiducial configuration is an appropriate choice for a CRF.

The mathematically optimal configuration of fiducial markers is an isotropic distribution where  $f_x = f_y = f_z$ . This can be realized by placing the fiducials at the vertices of a regular polyhedron, e.g., a regular tetrahedron for  $N = 4$ . In this case the expected squared TRE( $\mathbf{r}$ ) is described by

$$\langle \text{TRE}^2(\mathbf{r}) \rangle = \frac{\langle \text{FLE}^2 \rangle}{N} \left( 1 + \frac{2}{3} \frac{\rho^2}{r^2} \right) \quad (17)$$

where  $r$  is the distance of the fiducials from the fiducial centroid (i.e., the radius of the sphere circumscribing the regular polyhedron). Thus, the TRE at a point relative to an array of fiducials arranged in a regular polyhedron is not dependent on orientation. These results are summarized in Table II.

Finally, Fig. 3 shows two examples of the spatial distribution of tracking error of a surgical instrument relative to a CRF. These examples, which are applicable to cranial IGS, illustrate that: 1) For a particular instrument, the component of tracking error due to the instrument is constant, and in particular, is independent of the position and orientation of the instrument relative to the CRF. 2) The component of tracking error due to the CRF varies with the position of the instrument relative to the CRF.

3) The expected squared TRE for a serial composition of transformations, which is the case for tracking an instrument relative to a CRF, is the sum of the expected squared TREs for the individual transformations. Thus, the tracking errors of the two components add in quadrature.

### III. METHODS

#### A. Numerical Simulations

To test the correctness of (14), we perform numerical simulations and compare the TRE values produced by the simulations with those computed using (14). We perform the numerical simulations as follows (Fig. 4).

- 1) Pick CRF fiducial positions  $C_c^*$  such that fiducial centroid is at the origin. This can be accomplished for an existing set of CRF fiducial positions by subtracting fiducial centroid from each fiducial position.
- 2) Pick instrument fiducial positions  $F_i^*$  and instrument tip position  $\mathbf{p}_i^*$  such that tip position is at the origin. This can be accomplished for an existing set of instrument fiducial and tip positions by subtracting tip position from each fiducial position.
- 3) Place instrument tip at desired position relative to CRF by specifying translation vector  $\mathbf{t}_{ic}$ .
- 4) Simulate arbitrary instrument orientation by generating random rotation matrix  $R_{ic}$ .
- 5) Compute  $\mathbf{p}_c^* = \mathcal{T}_{ic}^*(\mathbf{p}_i^*)$  and  $F_c^* = \mathcal{T}_{ic}^*(F_i^*)$ , where  $\mathcal{T}_{ic}^*$  is composed of  $R_{ic}$  and  $\mathbf{t}_{ic}$ .
- 6) Simulate arbitrary OPS position and orientation by generating random transformation  $\mathcal{T}_{cp}^*$ .
- 7) Compute  $C_p^* = \mathcal{T}_{cp}^*(C_c^*)$ ,  $\mathbf{p}_p^* = \mathcal{T}_{cp}^*(\mathbf{p}_c^*)$ , and  $F_p^* = \mathcal{T}_{cp}^*(F_c^*)$ .
- 8) Simulate OPS fiducial measurement error by randomly perturbing each fiducial position in  $C_p^*$  and  $F_p^*$  to obtain  $C_p$  and  $F_p$ . Each fiducial position is isotropically perturbed by adding identical, independent, zero-mean, normally distributed noise with  $\sigma = \text{FLE} / \sqrt{3}$  to each  $x$ ,  $y$ , and  $z$  component.
- 9) Compute  $\mathcal{T}_{ip}$  by registering  $F_p$  and  $F_i^*$ . Compute  $\mathcal{T}_{pc}$  by registering  $C_p$  and  $C_c^*$ . The registration is performed by solving (1) using any of the registration methods cited in Section II-A. We use the method of Arun *et al.* [15].
- 10) Compute  $\mathbf{p}_c = \mathcal{T}_{pc}(\mathcal{T}_{ip}(\mathbf{p}_i^*))$ .
- 11) Compute  $\text{TRE}(\mathbf{p}_c) = |\mathbf{p}_c - \mathbf{p}_c^*|$ .
- 12) Perform 100 000 iterations of steps 4 to 11. Compute  $\text{rms}[\text{TRE}]$  as the rms average of the TRE values over all iterations.
- 13) Repeat steps 3 to 12 for various instrument tip positions relative to the CRF.

#### B. Experimental Measurements

We use a phantom of known geometry to perform experimental measurements. The phantom is a metal plate containing a set of conical divots arranged in a regular grid. The divots are spaced at 20-mm intervals, and their positions are machined with an accuracy of 0.025 mm. We use a  $4 \times 4$  grid subset of the divots. The phantom has a post that can be used to rigidly attach a CRF at various distances from the grid.

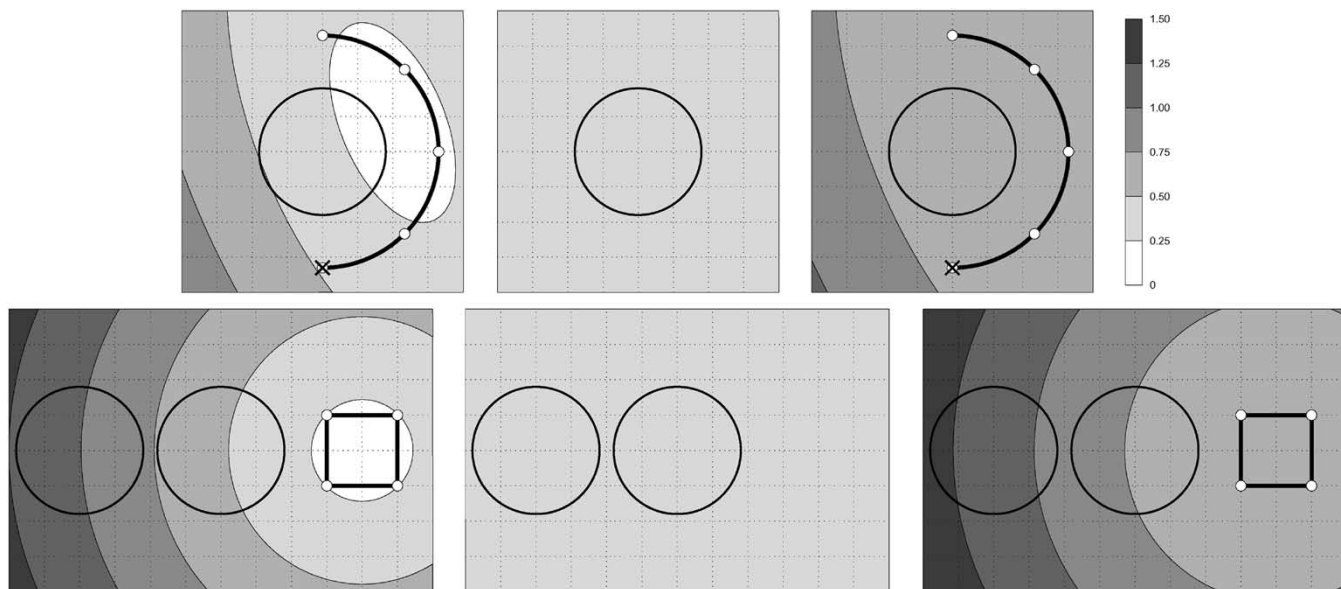


Fig. 3. Spatial distribution of tracking error of a surgical probe or instrument relative to a CRF. The left panels show the component of tracking error due to the CRF ( $TRE_{pc}$ ); tracking error is computed from (4) using the tip position relative to the CRF fiducials in the coordinate frame of the CRF. The middle panels show the component of tracking error due to the instrument ( $TRE_{ip}$ ); tracking error is computed from (4) using the tip position relative to the instrument fiducials in the coordinate frame of the instrument. The component of tracking error due to the instrument is constant, and in particular, is independent of the position and orientation of the instrument. For illustrative purposes, we arbitrarily chose an instrument with a tracking error of 0.5 mm. This could, for example, be an instrument with the fiducial configuration shown in Fig. 2(e) with  $\rho/A = 1.1$ ,  $\xi = B/A = 0.35$ , and  $FLE = 0.5$  mm. The instrument is not shown because the component of tracking error due to the instrument is independent of the position and orientation of the instrument. The right panels show the tracking error of the instrument relative to the CRF. The expected squared TRE for a serial composition of transformations, which is the case for tracking an instrument relative to a CRF, is the sum of the expected squared TREs for the individual transformations. Thus, the tracking errors of the two components are added in quadrature. The top and bottom row represent different CRFs. The head, which is approximated as a sphere of radius 90 mm and shown in these cross sections as a circle, is fixed in a head clamp. A CRF is rigidly connected to the head via a multijointed mechanical linkage that is attached to the head clamp (not shown). The CRF in the top row represents a CRF that is part of the StealthStation Treatment Guidance System (Medtronic Surgical Navigation Technologies, Louisville, CO) for cranial navigation. It consists of five IREDs (shown as small white circles) equally spaced on a semicircular arc of radius 165 mm. The tracking error due to this CRF was computed using only four of the IREDs assuming that one of the IREDs is not visible to the OPS (shown as small white circle with an  $\times$ ). The CRF in the bottom row represents a generic CRF that consists of four IREDs arranged in a square with side length 100 mm. Two heads are shown, representing two possible positions of the CRF relative to the head, one at 200 mm from the center of the head, the other at 400 mm from the center of the head. Tracking error was computed using an FLE value of 0.35 mm. Tracking error is color coded with six gray levels between 0 and 1.5 mm. A 50-mm dotted grid is provided for spatial reference.

The TRE value for a particular experiment is computed using the known geometry of the grid together with Sibson's result described by (3). An optically tracked probe with a 3-mm-diameter spherical tip is placed in each of the 16 divots and the probe tip positions reported by the tracking system are recorded. The set of measured probe tip positions is registered to the known (machined) divot positions. This process is repeated five times and the rms average of the FRE values obtained from the five registrations is computed. Sibson's result describes the statistical relationship among FRE, FLE, and  $N$ . The random component of tip tracking error in this experiment is analogous to FLE. Thus, we compute tip tracking error by rearranging (3) to

$$TRE_m = \sqrt{\frac{N}{N-2}} FRE \quad (18)$$

where  $TRE_m$  is the tip tracking error (the subscript " $m$ " denotes that the value of TRE is experimentally measured), FRE is the rms average of the FRE values obtained from the five registrations, and  $N = 16$  is the number of divot positions. For large values of  $N$ ,  $TRE_m \sim FRE$ . For  $N = 16$ ,  $\sqrt{N/(N-2)} \sim 1.069$ .

Two optical tracking systems were used in this study, an Optotrak 3020 and a Polaris. Both systems are manufactured by Northern Digital, Inc. (Waterloo, Ontario, Canada). These sys-

tems were chosen because they are used in several current commercially available IGS systems. The Optotrak 3020 is an active optical tracking system that tracks IREDs. The Polaris is manufactured in several models. The model used in this work is a hybrid active and passive optical tracking system that tracks both IREDs and RRSs. Both active and passive tracking are used. In the case of the Optotrak and Polaris using IREDs, we performed a standard pivot calibration using the Optotrak to calibrate the instrument tip. This calibration is performed by taking a large number of measurements (greater than 1000) while the instrument is pivoted about its spherical tip. The calibration is repeated at many positions in the working volume. For the Polaris system using RRSs, the instrument tip was set and verified by measurement at a machine shop.

The instrument fiducial configuration in these experiments is a rectangle as shown in Fig. 2(e). The instrument tracking fiducials are mounted on a metal plate. This plate can be variably positioned along a metal rod with a 3-mm-diameter spherical tip. The combination of the tracking fiducials, metal plate, and metal rod with spherical tip comprises our experimental optically tracked instrument. The CRF fiducial configuration is a square. The CRF fiducials are mounted on a metal plate that can be variably positioned along a post that is attached to the divot plate. Different instrument and CRF fiducial configuration dimensions are used for the Optotrak and Polaris systems. The in-

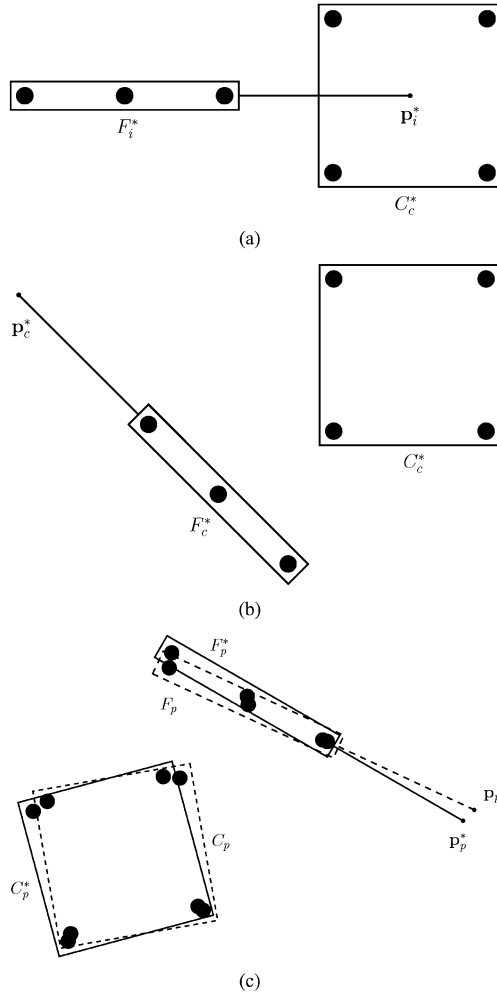


Fig. 4. Schematic illustration of the numerical simulation process. (a) The CRF fiducial positions, instrument tip position, and instrument fiducial positions are  $C_c^*$ ,  $p_c^*$ , and  $F_i^*$ , respectively (steps 1 and 2). (b) The true instrument tip position and instrument fiducial positions in the CRF coordinate system are  $p_c^*$  and  $F_c^*$ , respectively (steps 3 to 5). (c) The true CRF fiducial positions, instrument tip position, and instrument fiducial positions in the OPS coordinate system are  $C_p^*$ ,  $p_p^*$ , and  $F_p^*$ , respectively (steps 6 to 7). The OPS fiducial measurement error is simulated by randomly perturbing each fiducial position in  $C_p^*$  and  $F_p^*$  to obtain  $C_p$  and  $F_p$  (step 8).

instrument and CRF fiducials for the Optotrak system are arranged in a perfect rectangle and square, respectively. This is possible because the Optotrak system, unlike the Polaris system, strobes each IRED individually. The Polaris system has some fiducial asymmetry requirements. These requirements are due to the fact that in its active mode, the Polaris strobes sets of IREDs rather than each IRED individually, and in its passive mode, all RRSs are illuminated simultaneously. Thus, for the Polaris system, the fiducial positions were perturbed from the nominal rectangle (instrument) and square (CRF) configurations just enough to satisfy the asymmetry requirements.

For each optical tracking system, measurements are performed using two positions of the instrument fiducials relative to the spherical tip, two sizes of the CRF fiducial configuration, and four distances from the center of the divots to the centroid of the CRF fiducials. For each tracking system and experiment, the dimensions of the instrument fiducial configuration ( $A, B$ ),

the distance from the instrument tip to the centroid of the instrument fiducials ( $\rho$ ), the size of the CRF fiducial configuration ( $r$ ), and the distance from the center of the divots to the centroid of the CRF fiducial ( $d$ ) are listed in Table III. For the Optotrak system, the instrument fiducial configuration in these experiments is a rectangle. The column *Instrument* lists the values of the distance parameters  $\rho, A$ , and  $B$ , which are defined in Fig. 2(e). The CRF fiducial configuration is a square. The column *CRF* lists the dimension of the square; the value of the parameter  $r$  is the radius of the circle circumscribing the square. For the Polaris system, as mentioned above, the instrument and CRF fiducial configurations are nominally a rectangle and a square, respectively, with the fiducial positions perturbed sufficiently to satisfy the Polaris asymmetry requirements. In this case, the values of  $A, B$ , and  $r$  are the dimensions of the rectangle and circle that best fit the actual instrument and CRF fiducial configurations, respectively.

Three types of experiments were performed. In Experiment A, the instrument tip is placed in each divot with the instrument in a relatively constant orientation, and the divot plate and CRF are maintained in a fixed position relative to the optical tracking system. In Experiment B, the instrument orientation is randomly varied for each recorded divot position, but the divot plate and CRF are maintained in a fixed position. In Experiment C, for each recorded divot position, the instrument orientation is randomly varied, and the divot plate and CRF are randomly repositioned within the field of view (FOV) of the optical tracking system. The instrument and the CRF are kept stationary when the tracking data is collected (static data acquisition, in contrast to dynamic data acquisition reported by others [8], [10]).

In order to minimize angle-dependent FLE, active optical tracking data is used only if the angle formed by a line between the OPS and the IRED and a vector normal to the plane of the IRED is less than  $50^\circ$ . Measurements are made at the center of the OPS measurement volume. This is facilitated using custom software that displays the positions of the instrument and CRF fiducials on triplanar outlines of the OPS measurement volume. Also, the Polaris system has an “out-of-volume” zone where the system can measure fiducial positions but where the measurement error can be large. We avoid using such measurements by examining the out-of-volume flag provided by the system. For both the Optotrak and Polaris systems, we use measurements only if all four fiducials on both the instrument and the CRF are visible.

#### IV. RESULTS

We performed numerical simulations to estimate tip tracking error for a wide variety of instrument and CRF fiducial configurations and relative positions. For example, we computed the spatial distribution of tracking error shown in Fig. 3. For all simulations, we also computed the theoretically predicted values using (4) and (14). The differences between the simulation and theoretical values were generally less than 0.2%. The largest observed difference was 0.6%. Generally, the highest observed differences corresponded to cases with large  $d_k/f_k$  ratios. For the spatial distribution of tracking error shown in Fig. 3, the largest difference was less than 0.1%.

TABLE III  
COMPARISON OF THEORETICALLY PREDICTED AND EXPERIMENTALLY MEASURED TRACKING ERRORS

Tracking System/Mode	Instrument	CRF	$d$ (mm)	rms[TRE] (mm)				
				Theory	Expt. A	Expt. B	Expt. C	
Optotrak 3020/Active	$A = 50$ mm $B = 25$ mm $\rho = 75$ mm	$r = 28$ mm	100	0.36	0.22 (-38%)	0.35 (-3%)	0.22 (-39%)	
			200	0.62	0.23 (-63%)	0.37 (-40%)	0.58 (-6%)	
			300	0.89	0.39 (-56%)	0.54 (-40%)	1.37 (54%)	
			400	1.17	0.60 (-49%)	1.09 (-7%)	1.03 (-13%)	
	$A = 50$ mm $B = 25$ mm $\rho = 150$ mm	$r = 28$ mm	100	0.49	0.25 (-48%)	0.28 (-42%)	0.51 (5%)	
			200	0.70	0.34 (-51%)	0.56 (-19%)	1.00 (43%)	
			300	0.95	0.61 (-36%)	0.59 (-38%)	1.50 (58%)	
			400	1.22	0.72 (-41%)	0.63 (-48%)	1.77 (45%)	
	$A = 50$ mm $B = 25$ mm $\rho = 75$ mm	$r = 57$ mm	100	0.26	0.15 (-45%)	0.12 (-56%)	0.39 (47%)	
			200	0.36	0.14 (-62%)	0.35 (-5%)	0.21 (-42%)	
			300	0.49	0.19 (-60%)	0.51 (6%)	0.53 (10%)	
			400	0.62	0.43 (-30%)	0.49 (-21%)	0.78 (27%)	
	$A = 50$ mm $B = 25$ mm $\rho = 150$ mm	$r = 57$ mm	100	0.42	0.15 (-65%)	0.32 (-23%)	0.52 (23%)	
			200	0.49	0.36 (-26%)	0.49 (0%)	0.34 (-31%)	
			300	0.59	0.21 (-64%)	0.25 (-58%)	0.43 (-27%)	
			400	0.70	0.38 (-46%)	0.37 (-47%)	0.52 (-26%)	
	Polaris/Active	$A = 71$ mm $B = 54$ mm $\rho = 85$ mm	$r = 32$ mm	100	0.64	0.37 (-42%)	0.77 (20%)	1.05 (64%)
				200	1.10	0.62 (-44%)	0.48 (-56%)	1.16 (5%)
				300	1.60	1.22 (-24%)	1.11 (-31%)	2.83 (77%)
				400	2.11	0.66 (-69%)	2.31 (10%)	3.34 (58%)
		$A = 71$ mm $B = 54$ mm $\rho = 170$ mm	$r = 32$ mm	100	0.81	0.72 (-12%)	0.54 (-34%)	0.87 (7%)
				200	1.21	0.48 (-60%)	0.60 (-51%)	1.07 (-12%)
				300	1.68	0.91 (-46%)	0.90 (-46%)	2.34 (39%)
				400	2.17	1.09 (-50%)	1.93 (-11%)	2.95 (36%)
$A = 71$ mm $B = 54$ mm $\rho = 85$ mm		$r = 64$ mm	100	0.45	0.35 (-23%)	0.34 (-25%)	0.71 (56%)	
			200	0.64	0.22 (-66%)	0.72 (13%)	1.01 (58%)	
			300	0.86	0.33 (-62%)	0.94 (9%)	0.71 (-18%)	
			400	1.10	0.52 (-53%)	1.07 (-3%)	1.51 (37%)	
$A = 71$ mm $B = 54$ mm $\rho = 170$ mm		$r = 64$ mm	100	0.68	0.47 (-31%)	0.79 (16%)	0.64 (-6%)	
			200	0.81	0.75 (-8%)	0.55 (-32%)	0.53 (-35%)	
			300	1.00	0.54 (-46%)	0.44 (-56%)	1.09 (9%)	
			400	1.21	0.89 (-27%)	1.22 (1%)	1.19 (-2%)	
Polaris/Passive		$A = 71$ mm $B = 54$ mm $\rho = 85$ mm	$r = 35$ mm	100	0.87	0.45 (-48%)	0.82 (-6%)	0.95 (9%)
				200	1.46	0.75 (-49%)	1.50 (3%)	0.96 (-34%)
				300	2.11	1.58 (-25%)	1.55 (-26%)	3.06 (45%)
				400	2.77	2.64 (-5%)	2.69 (-3%)	3.85 (39%)
		$A = 71$ mm $B = 54$ mm $\rho = 170$ mm	$r = 35$ mm	100	1.14	0.66 (-42%)	1.17 (3%)	1.03 (-9%)
				200	1.63	1.30 (-20%)	2.01 (23%)	1.23 (-25%)
				300	2.23	1.79 (-20%)	2.21 (-1%)	2.72 (22%)
				400	2.86	1.47 (-49%)	2.16 (-25%)	2.95 (3%)
	$A = 71$ mm $B = 54$ mm $\rho = 85$ mm	$r = 71$ mm	100	0.64	0.60 (-6%)	0.78 (22%)	0.39 (-39%)	
			200	0.87	0.55 (-37%)	0.38 (-56%)	1.26 (45%)	
			300	1.15	0.94 (-19%)	1.24 (7%)	1.09 (-6%)	
			400	1.46	1.11 (-24%)	0.70 (-52%)	1.77 (21%)	
	$A = 71$ mm $B = 54$ mm $\rho = 170$ mm	$r = 71$ mm	100	0.97	0.54 (-45%)	0.74 (-24%)	1.23 (26%)	
			200	1.14	0.51 (-55%)	0.92 (-19%)	1.73 (52%)	
			300	1.37	1.29 (-6%)	1.19 (-13%)	1.96 (43%)	
			400	1.64	0.72 (-56%)	1.65 (1%)	1.92 (17%)	

For the Optotrak system, the instrument fiducial configuration in these experiments is a rectangle. The column *Instrument* lists the values of the distance parameters  $\rho$ ,  $A$ , and  $B$ , which are defined in Fig. 2(e). The CRF fiducial configuration is a square. The column *CRF* lists the dimension of the square; the value of the parameter  $r$  is the radius of the circle circumscribing the square. For the Polaris system, the instrument and CRF fiducial configurations are approximately a rectangle and a square, respectively (see text for additional detail). The column " $d$ " lists the distance from the center of the divots to the centroid of the CRF fiducials. The theoretical values of the individual components of tracking error were computed using Eq. (4); the tracking error of the instrument relative to the CRF, which is listed in the column *Theory*, was computed by adding the two components in quadrature according to Eq. (14). Theoretical values of the tracking error were computed for the Optotrak 3020, Polaris/Active, and Polaris/Passive using FLE values of 0.16, 0.33, and 0.48 mm, respectively. The three types of experiments (*Expt. A*, *B*, and *C*) and the computation of the experimental values of the tracking error are described in the text. The values in parentheses are differences, expressed as percentages, between experimental values and the corresponding theoretical values.

The experimental results are listed in Table III and plotted in Fig. 5. Corresponding theoretical values of the individual components of tracking error were computed using (4); the tracking

error of the instrument relative to the CRF was computed by adding the two components in quadrature according to (14). The rotational component of theoretical tracking error ranged

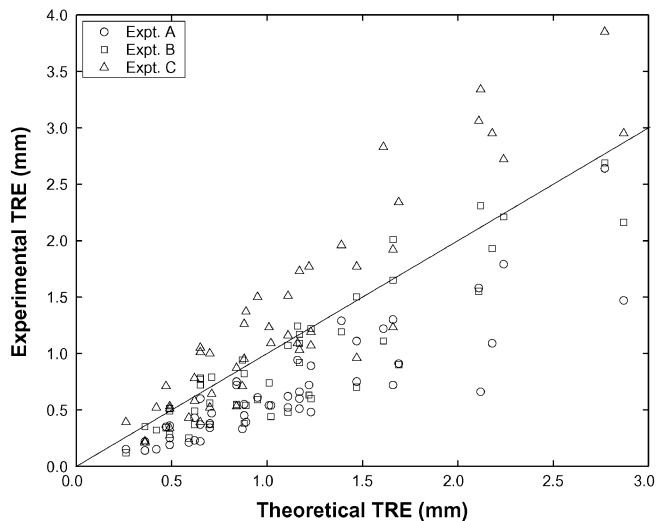


Fig. 5. Plot of experimentally measured versus theoretically predicted tracking errors. This plot is a graphical representation of all tracking error data listed in Table III. Identical experimental and theoretical tracking errors are represented by the diagonal line. The slopes of the regression lines of experimental vs. theoretical TRE for Experiments A, B, and C are 0.69, 0.90, and 1.33, respectively; the slope for all data pooled together is 0.97.

from 87% to 98% of total tracking error for the instruments and 82% to 99% for the CRFs. Theoretical values of the tracking error were computed for the Optotrak 3020, Polaris/Active, and Polaris/Passive using FLE values of 0.16, 0.33, and 0.48 mm, respectively. Each of these FLE values was determined using (3) and the rms average of all FRE values obtained from the corresponding optical tracking system during the tracking experiments. The differences between experimentally measured and theoretically predicted tip tracking errors are quite variable. The percentage difference varied from  $-69\%$  to  $-5\%$ ,  $-58\%$  to  $23\%$ , and  $-42\%$  to  $77\%$  for Experiments A, B, and C, respectively. Nonetheless, there is a strong correlation between experimental and theoretical TRE values as can be seen in Fig. 5. The correlation is significant ( $P < 0.001$ ) for Experiments A (correlation coefficient  $r = 0.87$ ), B ( $r = 0.90$ ), and C ( $r = 0.92$ ) and for all data pooled together ( $r = 0.82$ ). The slopes of the regression lines of experimental vs. theoretical TRE are considerably different for Experiments A (slope  $\beta = 0.69$ ), B ( $\beta = 0.90$ ), and C ( $\beta = 1.33$ ); the slope for all data pooled together is  $\beta = 0.97$ . For each tracking system and experiment, there are three variables: distance from the instrument tip to the instrument fiducials ( $\rho$ ), size of the CRF fiducial configuration ( $r$ ), and distance from the divots (instrument tip) to the CRF fiducials ( $d$ ). Although there is considerable variability in the experimental results, overall the experimentally measured tracking error increased, as theoretically predicted, as  $\rho$  increased,  $r$  decreased, and  $d$  increased.

## V. DISCUSSION

Instrument tip tracking errors theoretically predicted by (4), (5), and (14) are in excellent agreement with values obtained by numerical simulation for the wide variety of instrument and CRF fiducial configurations and relative positions that we tested, both in this and previous [1] work. It is possible to

perform numerical simulations to test candidate fiducial configurations. One advantage of theory compared to simulation is that it provides valuable insights and enables the derivation of useful relationships among important variables such as (4), (5), and (14) and the formulas in Tables I and II.

The theoretical results in this paper assume that FLE, which is the fiducial position measurement error, is identical, independent, zero-mean, and isotropic. For optical tracking systems, FLE is generally slightly anisotropic, with error along the optical axis of the OPS higher than the error perpendicular to this axis. This is fundamentally due to the fact that the distance from the sensors to the tracking fiducial markers is substantially larger than the distance between the sensors in the OPS. Also, the optical center of IREDs used for active optical tracking is slightly angle dependent and, thus, FLE depends on the angle formed by a line between the OPS and the IRED and a vector normal to the IRED. If the IREDs on an instrument or CRF are coplanar with identical unit normals, then the angle-dependent component of FLE is correlated. For the OPS systems used in this study, the angle-dependent error becomes substantial for angles higher than  $60^\circ$  [32]. In order to minimize angle-dependent FLE, active optical tracking data was used only if the angle formed by a line between the OPS and the IRED and a vector normal to the plane of the IRED was less than  $50^\circ$ . One component of FLE is temporal variation, sometimes called “jitter,” which is caused by factors such as thermal noise. This component appears to be very random. We made some measurements of temporal variation and found that this component of FLE is  $<0.05$ ,  $\sim 0.05$ – $0.1$ , and  $\sim 0.1$ – $0.2$  mm for the Optotrak 3020, Polaris/Active, and Polaris/Passive systems, respectively, which is approximately 20%–40% of total FLE. These measurements are comparable to previously reported values [9]. Jitter can be reduced by averaging sequential measurements [33], but only single measurements were made in this study. Another component of FLE is spatial variation. Imperfections in the OPS such as nonideal lenses cause spatial distortion in the FOV that cannot be fully corrected for by the OPS calibration process. This component is pseudo-random, in the sense that measurements at different positions in the FOV appear to be random, but repeated measurements at the same position will have the same position-dependent component of FLE.

One purpose of Experiments A, B, and C was to examine the importance of angle-dependent and position-dependent components of FLE. Since the instrument and CRF fiducials were coplanar, there was some correlated error in all experiments. In Experiment A, the instrument tip was placed in each divot with the instrument in a relatively constant orientation, and the divot plate and CRF were maintained in a fixed position relative to the OPS. Thus, in this experiment the angle-dependent component of FLE was relatively constant for the instrument, and the angle-dependent and position-dependent components of FLE were relatively constant for the CRF. In Experiment B, the instrument orientation was randomly varied for each recorded divot position, but the divot plate and CRF were maintained in a fixed position. Thus, in this experiment the angle-dependent component of FLE was more random for the instrument than in Experiment A. In Experiment C, for each recorded divot position, the instrument orientation was randomly varied, and

the pivot plate and CRF were randomly repositioned within the FOV of the optical tracking system. Thus, in this experiment the angle-dependent component of FLE was more random for the instrument than in Experiment A, and the angle-dependent and position-dependent components of FLE were more random for the CRF than in Experiments A and B. Since the experimental method in this work measures only the random component of tracking error, it is not surprising that the measured tracking error was smallest in Experiment A (smallest slope of the regression line of experiment vs. theoretical TRE values) and largest in Experiment C. The results of Experiment C are probably more accurate measurements of true tracking error than those of A and B. The observation that the measured tracking error in Experiments A and B, which do not include some angle- and position-dependent components of error, was considerably smaller than in Experiment C suggests that these components of error are important, as has been noted by others [8], [10]. Nonetheless, the discussion in this paragraph is merely one explanation of observed trends in the experimental measurements.

We used two optical tracking systems in this work, and one of the systems in two different modes of operation, namely active tracking of IREDs and passive tracking of RRSs. The theoretical TRE values for the experimental measurements varied from 0.3 to 2.9 mm, i.e., by one order of magnitude. Over this range, for the three optical tracking systems/modes, there is a strong and significant correlation between experimental and theoretical TRE values (Fig. 5). And, overall, the experimentally measured tracking error increased, as theoretically predicted, as the distance from the instrument tip to the instrument fiducials increased, the size of the CRF fiducial configuration decreased, and the distance from the divots (instrument tip) to the CRF fiducials increased. These observations lead us to conclude that although some of the assumptions of the point-based registration error theory used in this paper are only approximately true, and although the differences between experimentally measured and theoretically predicted tip tracking errors are quite variable, with a maximum observed difference of 77% (Table III), the theoretical results presented in this paper produce sufficiently accurate predictions to be practically useful and provide a valuable framework for understanding and analyzing the effect of fiducial marker configuration on tip position tracking error.

The theoretical results in this paper may be useful for the design of optically tracked instruments for IGS. There are many issues that influence the design of such instruments (e.g., ergonomics, sterilizability, manufacturing cost). This paper is concerned with the effect of fiducial marker configuration on tip position tracking error. Tip position tracking error decreases as the distance from the instrument tip to the instrument fiducials decreases and as the distance between the fiducials along the axis of the tool increases. If a CRF is used to define an intraoperative coordinate system in which the tip position is reported, tracking error decreases as the distance between the instrument tip and the CRF fiducials decreases and as the distance between the CRF fiducials increases. As an example of the application of the theoretical results, consider the design of a CRF for cranial navigation. Assume that a planar configuration of four IREDs is being considered, that the IRED localization error (FLE) of the OPS being used is 0.35 mm, and

that one of the design requirements is that the component of tracking error due to the CRF must be less than 0.5 mm when the CRF is placed at a distance of 200 mm from the head. Using (16) for the worst case of  $\phi = \pi/2$ , which is listed in Table II, and approximating the error by its rotational component

$$r \geq \sqrt{\frac{4}{3N}} \frac{\text{FLE}}{\text{TRE}_{\max}} \rho \quad (19)$$

which is approximately  $r \sim 80$  mm, or equivalently, the length of the side of the square must be approximately  $r\sqrt{2} \sim 115$  mm. This is similar to the example in the bottom row of Fig. 3, which shows a CRF that consists of four IREDs in a square with side length 100 mm, except that the best case of  $\phi = 0$  is illustrated. However, because there is considerable variability in the relationship between experimentally measured and theoretically predicted tip tracking error (Fig. 5), fiducial configurations developed using the theory presented in this paper need to be carefully tested to ensure that they produce the desired level of accuracy. Also, the experimental verification of the theoretical results was carefully performed in a laboratory. During clinical use in a surgical environment, optical tracking accuracy can be degraded in several ways. One important source of error is shift in the measured position of the fiducial markers. This can be caused by partial blockage of the fiducial markers by other instruments. For reflectors (RRSs), this can be caused by blood spots on the reflector.

The result in (4) suggests that the statistically expected value of TRE is inversely proportional to  $\sqrt{N}$ . This is true only if fiducials are added to the configuration such that their rms distance to the three principal axes ( $f_k$ ) remains constant. Given a configuration of  $N$  fiducials, placing an additional fiducial at the fiducial centroid improves the translational component of TRE but does not change the rotational component, which is generally the dominant component for surgical instruments and tools. The denominator of each of the rotational component terms is  $Nf_k^2 = \sum_i f_{ik}^2$ , where  $f_{ik}$  is the distance of the  $i$ th fiducial from the  $k$ th principal axis. The summation  $\sum_i f_{ik}^2$  does not change if an additional fiducial is placed at the fiducial centroid. For example, consider instruments (a) and (b) in Fig. 2 and Table I. The instrument with three equally spaced collinear fiducial markers has the identical rotational component of tracking error as the instrument with two collinear fiducials.

Sometimes one is interested in the tracking error not only at the tip of the instrument but everywhere in the FOV of the instrument, e.g., an endoscope or an ultrasound probe. Fig. 6 shows the spatial distribution of statistically expected tracking error in an instrument's FOV for five different fiducial configurations. The distribution in the FOV along the instrument's axis is important if a virtual extension of the instrument tip along the axis is used in the IGS system (e.g., to plan a biopsy trajectory or guide a drill).

A commonly asked question in the design of CRFs is how much improvement in accuracy is achieved by distributing the fiducial markers in a volume rather than in a plane. One way of addressing this question is to compute the ratio of the tracking errors for two fiducial configurations, one where the fiducial markers are placed at the vertices of a regular polyhedron

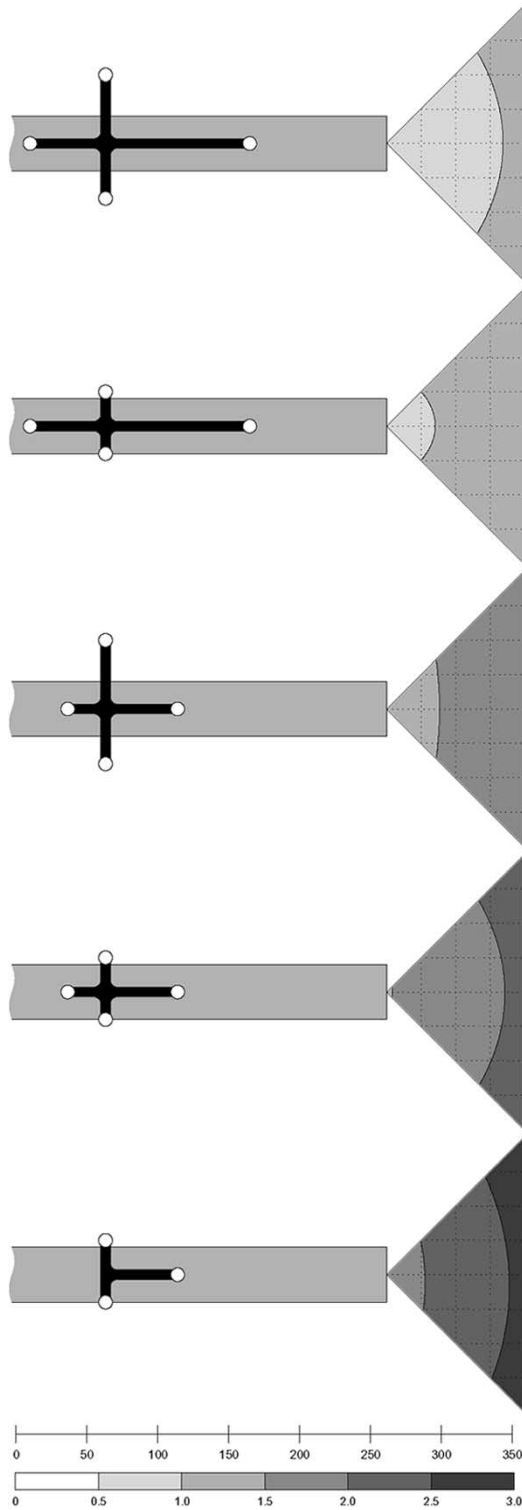


Fig. 6. Statistically expected tracking error in an instrument's FOV up to 100 mm from the instrument tip. The spatial distribution of tracking error is shown for five different fiducial configurations. The instrument could be an endoscope or an ultrasound probe for which one is interested in the tracking error not only at the instrument tip but everywhere in the FOV. Tracking error was computed using (4) for each point  $\mathbf{r}$  in the FOV using an FLE value of 0.5 mm. The first grid at the bottom is a distance scale in units of millimeters; the distance between grid lines in the FOV is 25 mm. The second grid at the bottom is a tracking error scale; tracking error in the FOV is color coded with six gray levels between 0 and 3 mm.

("3-D"), and one where the fiducials are placed at the vertices of a regular polygon [two-dimensional ("2-D")] located on a

great circle of the sphere circumscribing the polyhedron. This ratio is obtained by dividing (16) by (17)

$$\frac{\text{rms}[\text{TRE}(\mathbf{r})]_{2\text{-D}}}{\text{rms}[\text{TRE}(\mathbf{r})]_{3\text{-D}}} = \sqrt{\frac{1 + \frac{3 + \sin^2 \phi}{3} \frac{\rho^2}{r^2}}{1 + \frac{2}{3} \frac{\rho^2}{r^2}}} \sim \sqrt{\frac{3 + \sin^2 \phi}{2}} \quad (20)$$

where the approximation assumes values of  $\rho/r$  much greater than 1. This ratio varies from  $\sqrt{3/2} \sim 1.22$  for  $\phi = 0$  to  $\sqrt{2} \sim 1.41$  for  $\phi = \pi/2$ . Thus, the tracking error of an optimal 2-D configuration (e.g., square) is about 22% higher than that of an optimal 3-D configuration (e.g., tetrahedron) when navigating in the plane of the CRF ( $\phi = 0$ ), and about 41% higher when navigating perpendicular to the plane ( $\phi = \pi/2$ ).

This paper is concerned with the effect of fiducial marker configuration on tip position tracking error. In addition to displaying the tip position of a surgical probe or instrument on reformatted or rendered preoperatively acquired images of the patient, many IGS systems also display the orientation of the instrument. The theoretical results in this paper can be easily extended to include orientation tracking error. The total rotational component of TRE is given in (15). The component of TRE due to rotation about the  $k$ th principal axis is

$$\langle \text{TRE}^2(\mathbf{r}) \rangle_{\text{rotation},k} = \frac{\langle \text{FLE}^2 \rangle}{3N} \frac{d_k^2}{f_k^2} = d_k^2 \langle (\Delta\theta_k)^2 \rangle \quad (21)$$

and, thus, the rotation angle error about the  $k$ th principal axis is

$$\text{rms}[\Delta\theta_k] = \frac{\text{FLE}}{\sqrt{3N} f_k}. \quad (22)$$

Optically tracked instruments, such as those shown in Fig. 2, tend to have fiducial configurations with considerable anisotropy. In particular,  $f_x$  is generally zero or small, where  $x$  is the principal axis corresponding to the axis of the instrument. Generally the primary concern is tracking the tip of the instrument. Since the tip is either on or near the  $x$  axis, the ratio  $d_x/f_x$  is either zero or small and tip tracking accuracy can be relatively good. However, as can be seen from (22), a small value of  $f_x$  will produce a high rotational error about the axis of the instrument ( $\Delta\theta_x$ ). This is an important design consideration in applications such as image-enhanced endoscopy [34] where the "twist" of the instrument (i.e., the rotation angle about the axis of the instrument) is a critical orientation parameter measured and reported by the tracking system. Rotational error about the instrument axis can be reduced by increasing the distribution of fiducials perpendicular to this axis (which increases  $f_x$ ). The trajectory error ( $\Delta\theta_y, \Delta\theta_z$ ) of an instrument is also important in some applications, for example, the positioning of a pedicle screw for posterior spinal fixation. Trajectory error can be reduced by increasing the distribution of fiducials along the instrument axis (which increases  $f_y$  and  $f_z$ ). It should be emphasized, however, that the experimental results reported in this paper verified only theoretical instrument tip position tracking error. The validity of expected instrument orientation error theoretically predicted by (22) still needs to be experimentally verified and will be the subject of future work.

## ACKNOWLEDGMENT

The authors would like to thank the anonymous reviewers and the following individuals for their many helpful comments and suggestions: J. M. Fitzpatrick (Vanderbilt University, Nashville, TN); D. Crouch and G. Mosher (Northern Digital, Inc., Waterloo, ON, Canada); R. Khadem, R. Randall, and J. Ho (CBYON, Inc., Mountain View, CA); D. Simon and A. Bzostek (Medtronic Surgical Navigation Technologies, Louisville, CO); K. Mori (Nagoya University, Nagoya, Japan); and R. Shahidi (Stanford University, Stanford, CA). The authors gratefully acknowledge M. Bax (Stanford University, Stanford, CA) for helping create the illustrations in Figs. 3 and 6.

## REFERENCES

- [1] J. B. West and C. R. Maurer Jr., "The extension of target registration error theory to the composition of transforms," *Proc. SPIE (Medical Imaging 2002: Image Processing)*, vol. 4684, pp. 574–580, 2002.
- [2] P. DiMatteo, P. Rademacher, and H. Stern, "Method of Sensing the Position and Orientation of Elements in Space," U.S. Patent 4 396 945, Aug. 2, 1983.
- [3] E. Alexander, III and R. J. Maciunas, Eds., *Advanced Neurosurgical Navigation*. New York: Thieme Medical, 1999.
- [4] I. M. Germano, Ed., *Advanced Techniques in Image-Guided Brain and Spine Surgery*. New York: Thieme, 2002.
- [5] P. L. Gildenberg and R. R. Tasker, Eds., *Textbook of Stereotactic and Functional Neurosurgery*. New York: McGraw-Hill, 1998.
- [6] R. H. Taylor, S. Lavalley, G. Burdea, and R. Mösges, Eds., *Computer-Integrated Surgery: Technology and Clinical Applications*. Cambridge, MA: MIT Press, 1996.
- [7] C. R. Maurer Jr., T. Rohlfing, D. Dean, J. B. West, D. Rueckert, K. Mori, R. Shahidi, D. P. Martin, M. P. Heilbrun, and R. J. Maciunas, "Sources of error in image registration for cranial image-guided surgery," in *Advanced Techniques in Image-Guided Brain and Spine Surgery*, I. M. Germano, Ed. New York: Thieme, 2002, pp. 10–36.
- [8] F. Chassat and S. Lavalley, "Experimental protocol of accuracy evaluation of 6-D localizers for computer-integrated surgery: Application to four optical localizers," in *Lecture Notes in Computer Science*, vol. 1496, Proc. 1st Int. Conf. Medical Imaging Computing and Computer-Assisted Intervention (MICCAI'98), W. M. Wells III, A. C. F. Colchester, and S. L. Delp, Eds, Berlin, 1998, pp. 277–284.
- [9] R. Khadem, C. C. Yeh, M. Sadeghi-Tehrani, M. R. Bax, J. A. Johnson, J. N. Welch, E. P. Wilkinson, and R. Shahidi, "Comparative tracking error analysis of five different optical tracking systems," *Comput. Aided Surg.*, vol. 5, pp. 98–107, 2000.
- [10] S. Schmerber and F. Chassat, "Accuracy evaluation of a CAS system: Laboratory protocol and results with 6D localizers, and clinical experiences in otorhinolaryngology," *Comput. Aided Surg.*, vol. 6, pp. 1–13, 2001.
- [11] J. M. Fitzpatrick, J. B. West, and C. R. Maurer Jr., "Predicting error in rigid-body, point-based registration," *IEEE Trans. Med. Imag.*, vol. 17, pp. 694–702, Oct. 1998.
- [12] C. R. Maurer Jr., G. B. Aboutanos, B. M. Dawant, R. J. Maciunas, and J. M. Fitzpatrick, "Registration of 3-D images using weighted geometrical features," *IEEE Trans. Med. Imag.*, vol. 15, pp. 836–849, Dec. 1996.
- [13] P. H. Schönemann, "A generalized solution of the orthogonal Procrustes problem," *Psychometrika*, vol. 31, pp. 1–10, 1966.
- [14] G. H. Golub and C. F. van Loan, *Matrix Computations*. Baltimore, MD: The Johns Hopkins Univ. Press, 1983.
- [15] K. S. Arun, T. S. Huang, and S. D. Blostein, "Least-squares fitting of two 3-D point sets," *IEEE Trans. Pattern Anal. Machine Intell.*, vol. PAMI-9, pp. 698–700, 1987.
- [16] S. Umeyama, "Least-squares estimation of transformation parameters between two point patterns," *IEEE Trans. Pattern Anal. Machin. Intell.*, vol. 13, pp. 376–380, Apr. 1991.
- [17] V. R. Mandava, "Three dimensional multimodal image registration using implanted markers," Ph.D. dissertation, Vanderbilt Univ., Nashville, TN, 1991.
- [18] O. D. Faugeras and M. Hebert, "The representation, recognition, and locating of 3-D objects," *Int. J. Robot. Res.*, vol. 5, pp. 27–52, 1986.
- [19] M. Froimowitz and S. Matthyse, "Geometrical correspondence between phenazocine and the enkephalins," *J. Med. Chem.*, vol. 29, pp. 573–578, 1986.
- [20] B. K. P. Horn, "Closed-form solution of absolute orientation using unit quaternions," *J. Opt. Soc. Amer. A, Opt. Image Sci.*, vol. 4, pp. 629–642, 1987.
- [21] B. F. Green, "The orthogonal approximation of an oblique structure in factor analysis," *Psychometrika*, vol. 17, pp. 429–440, 1952.
- [22] B. K. P. Horn, H. M. Hilden, and S. Negahdaripour, "Closed-form solution of absolute orientation using orthonormal matrices," *J. Opt. Soc. Amer. A, Opt. Image Sci.*, vol. 5, pp. 1127–1135, 1988.
- [23] M. W. Walker, L. Shao, and R. A. Volz, "Estimating 3-D location parameters using dual number quaternions," *CVGIP: Image Understanding*, vol. 54, pp. 358–367, 1991.
- [24] D. W. Eggert, A. Lorusso, and R. B. Fisher, "Estimating 3-D rigid body transformations: A comparison of four major algorithms," *Machine Vis. Applicat.*, vol. 9, pp. 272–290, 1997.
- [25] C. R. Maurer Jr., J. M. Fitzpatrick, M. Y. Wang, R. L. Galloway Jr., R. J. Maciunas, and G. S. Allen, "Registration of head volume images using implantable fiducial markers," *IEEE Trans. Med. Imag.*, vol. 16, pp. 447–462, Aug. 1997.
- [26] J. B. West, J. M. Fitzpatrick, S. A. Toms, C. R. Maurer Jr., and R. J. Maciunas, "Fiducial point placement and the accuracy of point-based, rigid-body registration," *Neurosurgery*, vol. 48, pp. 810–817, 2001.
- [27] R. Sibson, "Studies in the robustness of multidimensional scaling: Perturbational analysis of classical scaling," *J. Roy. Statist. Soc. B*, vol. 41, pp. 217–229, 1979.
- [28] J. M. Fitzpatrick and J. B. West, "Distribution of target registration error in rigid-body point-based registration," *IEEE Trans. Med. Imag.*, vol. 20, pp. 917–927, Sept. 2001.
- [29] K. Darabi, P. Grunert, and A. Perneczky, "Analysing the relationship between fiducial position and the geometrical error of intraoperative navigation," *Comput. Aided Surg. (Abstract from the conference Computer Integrated Surgery 1997)*, vol. 2, p. 224, 1997.
- [30] A. C. Evans, S. Marrett, D. L. Collins, and T. M. Peters, "Anatomical-functional correlative analysis of the human brain using three dimensional imaging systems," *Proc. SPIE (Medical Imaging III: Image Processing)*, vol. 1092, pp. 264–274, 1989.
- [31] D. L. G. Hill, D. J. Hawkes, M. J. Gleeson, T. C. S. Cox, A. J. Strong, W.-L. Wong, C. F. Ruff, N. D. Kitchen, D. G. T. Thomas, J. E. Crossman, C. Studholme, A. J. Gandhe, S. E. M. Green, and G. P. Robinson, "Accurate frameless registration of MR and CT images of the head: Applications in surgery and radiotherapy planning," *Radiology*, vol. 191, pp. 447–454, 1994.
- [32] A. T. Johnston, "Non-Isotropic Behavior of Active Infrared Markers (Tested With the Polaris System)," Northern Digital, Inc., Waterloo, ON, Canada, Tech. Rep. NDI-TR-0133, Jan. 1999.
- [33] J. B. West, R. Khadem, and C. R. Maurer Jr., "A nonlinear averaging method to optimize the accuracy of optical tracking," *Proc. SPIE (Medical Imaging 2003: Visualization, Image-Guided Procedures, Display)*, vol. 5029, pp. 311–318, 2003.
- [34] R. Shahidi, M. R. Bax, C. R. Maurer Jr., J. A. Johnson, E. P. Wilkinson, B. Wang, J. B. West, M. J. Citardi, K. H. Manwaring, and R. Khadem, "Implementation, calibration, and accuracy testing of an image-enhanced endoscopy system," *IEEE Trans. Med. Imag.*, vol. 21, pp. 1524–1535, Dec. 2002.